Re-examining the Role of Subsurface Oxygen Vacancies in the Dissociation of H_2O Molecules on Anatase TiO_2

Authors

Kolade Augustine Oyekan[1], Maarten Van de Put[1], Sabyasachi Tiwari[1], Carole Rossi[2], Alain Esteve[2], William Vandenberghe[1,*]

[1]Department of Materials Science and Engineering, The University of Texas at Dallas, RL10
800 West Campbell Road Richardson, TX 75080 USA

[2] LAAS-CNRS, University of Toulouse, 7 avenue du colonel Roche, 31031 Toulouse, France

*Corresponding Author

William Vandenberghe: william.vandenberghe@utdallas.edu

Abstract

Titanium (IV) oxide is a reference photocatalytic material for a number of chemical processes of interest in the energy transition, including the reduction of water into hydrogen gas. Density functional theory calculations have previously revealed that the decomposition into hydrogen and hydroxyl ions could be catalyzed by a subsurface oxygen vacancy (V_O). However, these theoretical investigations have been carried out with models considering only isolated water molecules. We investigate the role of the subsurface V_O at different levels of coverage up to full monolayer (ML) coverage. We observe that migration of the vacancy concomitantly to water decomposition is mandatory to obtain an exothermic pathway. Furthermore, the migration of the V_O only occurs in the presence of an under-coordinated surface oxygen atom. As coverage and decomposition increase, surface oxygen atoms are saturated which inhibit further migration of the subsurface V_O; hence the V_O shows no catalytic effect on the splitting of water into hydrogen and hydroxyl ions at full water coverage.

Keywords: DFT, Anatase TiO_2, Oxygen vacancy, Water dissociation, Full coverage, Hydrogen

1. Introduction

Titanium (IV) oxide (TiO_2) is arguably one of the most investigated semiconductor materials due to its exquisite physical and chemical properties and consequent numerous applications [1]. Among other metal oxides, TiO_2's chemical stability, low toxicity, environmentally friendly nature, and reusability, have led to its widely accepted consideration as a top leading photocatalyst [2], particularly since the seminal work by Honda and Fukushima in 1973 [3], which paved the way to photoelectrochemical materials and systems for hydrogen production through the splitting of water molecules. Since then, much effort has been focused on overcoming the TiO_2 weaknesses, such as the high electron/hole recombination rate and its optical absorption limited to the UV region, in both theoretical (mostly density functional theory, DFT) and experimental communities [4–6]. While several experimental research routes including doping [7–9], heterojunctions with other semiconductors [10], and embedding of plasmonic nanoparticles [4,11] have been pursued, DFT calculations have concentrated on surface chemistry for a number of applications and associated molecular decomposition of probe molecules such as methanol, ethanol, and water [12–16], which is the focus of the present article.

TiO_2 has three stable polymorphs: rutile, anatase, and brookite. Rutile and anatase are widely studied for catalytic applications, but anatase has been shown to be more photo-reactive, and it is also the most stable form found in nanocrystals [17,18] . For these reasons, anatase is the most utilized form of TiO_2 in photocatalytic applications, and consequently in DFT-based investigations. The (101) surface of anatase was established to be the most stable one [17–19], and this has led to a number of DFT investigations dedicated to the water splitting process [12,14,15,20].

Results from the literature indicate that the limiting step in the dissociation of a single water molecule on the anatase (101) surface lies on the ability of an adsorbed water molecule to decompose into an adsorbed hydroxyl group and a hydrogen ion in solution [21]. In the calculations by Aschauer and co-workers, the activation barrier of this step for a single water molecule on a pristine anatase (101) surface is 0.52 eV, and the overall endothermic reaction energy is 0.38 eV, making it thermodynamically unfavorable. [14]. Interestingly, studies have shown that the dissociation process can be enhanced by the presence of an oxygen vacancy in the anatase slab [12,14,15], and many studies have reported that a subsurface vacancy has a lower formation energy than a surface vacancy [22,23]. Rather than a surface vacancy, a defective slab with a subsurface oxygen vacancy led to a reduced kinetic barrier (by 0.26 eV), relative to a stoichiometric slab, but the water dissociation process was shown to remain thermodynamically unfavorable (by 0.32 eV). Experiments at low temperature and pressure on

a defective slab with subsurface defects also indicate higher binding energies for water on a defective slab, compared to a pristine slab [14]. In contrast, some results from the literature, including the present study, show that not only is the kinetic barrier reduced, but the overall reaction becomes thermodynamically favorable in the presence of a subsurface oxygen vacancy [12,15].

However, it is well documented that molecular water adsorption is exothermic [16,20,24,25] and that it is thermodynamically favorable for the surface to be completely covered with chemisorbed water molecules in their molecular form. The effect of defective surfaces has been explored to a lesser extent, while being of much technological importance. In particular, DFT studies examining the effect of subsurface V_O have only dealt with a single or sparse concentration of water molecules on the anatase (101) surfaces. Importantly, it was reported that the enhanced dissociation in the presence of a subsurface oxygen vacancy is accompanied by the migration of the vacancy towards the surface [12,15], leading to its annihilation. As a result, the exact role of the vacancy defect in the photocatalysis of water on the TiO_2 anatase (101) surface requires further investigation. It is also important to investigate the issue of the impact of water coverage on the dissociation chemistry when considering defective TiO_2.

In this work, we study theoretically water dissociation on defective anatase (101) accounting for full water coverage. Using DFT, we investigate and compare the dissociation of water molecules on a perfect and a defective surface at different levels of coverage: from a minimum coverage of 17% up to 100% (1 ML coverage). We examine the behavior of the subsurface oxygen vacancy during dissociation. Our results indicate that dissociation of adsorbed water molecules on a defective surface is exothermic up to 67% coverage (2/3 ML). At higher, more realistic, coverage the dissociation becomes endothermic, similar to the endothermic dissociation obtained for a perfect surface at all levels of coverage. Therefore, we thus find that the V_O has no catalytic effect on the splitting of water into hydrogen and hydroxyl ions on a defective anatase (101) surface at high coverage.

2 Method

2.1 DFT Calculations

We performed spin-polarized DFT calculations using the generalized gradient approximation (GGA) with the Perdew-Burke-Ernzehof (PBE) [26] exchange-correlation potential as implemented in the Vienna ab-Initio Simulation Package (VASP) [27–30]. Ion-electron interactions were described by projector augmented waves (PAW) pseudopotentials [31,32], and the electron wave functions were expanded in terms of plane wave basis sets, with a kinetic energy cutoff of 400 eV. Wavefunctions were optimized until the change in total energy was less than 10^{-6} eV. We employed Grimme's DFT-D3 method to include dispersion contributions to

the energy values [33]. Potential energy surfaces to determine the kinetic barrier were calculated using the nudged elastic band (NEB) method [34].

The anatase (101) surface supercell is built from a three-layer geometry (see Fig. 1), with a vacuum of 10 Å between slabs along the direction normal to the surface. The 1 x 3 surface supercell measuring 10.376 x 11.256 $Å^2$ has a total of 108 atoms. The bottom layer of TiO_2 was fixed while all other atoms were allowed to relax in all directions during minimization of the total energy. Due to the large size of the supercell, the Brillouin zone was sampled at the gamma point only. The unit cell from which the surface slab is cut was relaxed using a kinetic energy cutoff of 520 eV, and the lattice parameters obtained are: a = b = 3.8073 Å, c = 9.7318 Å, which are in good agreement with values from other computational and experimental studies [35,36].

2.2 Anatase TiO_2 model surfaces

The stoichiometric anatase (101) surface slab is shown in Fig. 1. It has a saw tooth-like morphology, with rows of fully coordinated (Ti_{6c}) and under coordinated (Ti_{5c}) Ti atoms along the [010] direction. These rows of Ti atoms are joined by three-fold coordinated (O_{3c}) and two-fold coordinated (O_{2c}) oxygen atoms. Water molecules are most easily adsorbed on the Ti_{5c} atoms, and for the 1 x 3 supercell used in the calculations, there are six such Ti_{5c} sites (two rows of 3 Ti_{5c}).

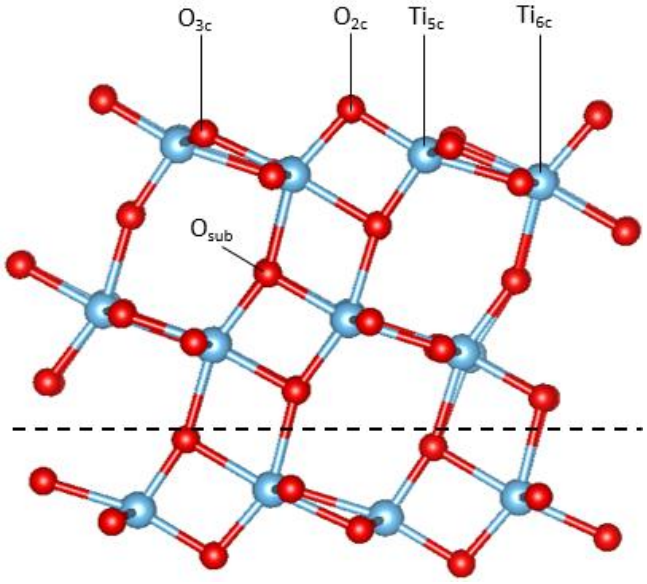

Figure 1: Side view of the 1 x 3 anatase (101) slab. Titanium atoms are cyan while oxygen atoms are red. O_{sub} is the oxygen atom removed to create the subsurface vacancy in the defective surface. Atoms underneath the dashed line are held fixed during minimizations of the total energy.

The single oxygen vacancy defective surface slab was obtained by removing the oxygen atom labelled O_{sub} in Fig. 1. Previous studies, both experimental and theoretical, have established that the subsurface vacancy created by removing O_{sub} has a lower formation energy than the most stable surface vacancy created by removing O_{2c} , or other subsurface oxygen sites [23,37,38].

2.3 Adsorption Energy Calculations

An incremental energy needed for the molecular adsorption of the nth water molecule on each surface, $\Delta E_{ads,n}$ is defined as:

$$\Delta E_{ads,n} = E_{slab}(nH_2O) - E_{slab}((n-1)H_2O) - E^{\infty}_{H_2O} \qquad (1)$$

where n = 6 means full coverage. $E_{slab}(nH_2O)$ and $E_{slab}((n-1)H_2O)$ are the total energies of a slab supercell containing *n* and *(n-1)* adsorbed water molecules, respectively. $E^{\infty}_{H_2O}$ is the total energy of an isolated water molecule, as being positioned at an infinite position from the surface, in vacuum. A negative value of $\Delta E_{ads,n}$ indicates an exothermic process, while a positive value indicates an endothermic process.

The molecular adsorption energy per molecule is given by:

$$\bar{E}_{ads} = \frac{E_{slab}(nH_2O) - E_{slab} - n \times E^{\infty}_{H_2O}}{n} \qquad (2)$$

where E_{slab} is the total energy of a surface slab, and n is the number of water molecules adsorbed on the surface. The dissociative adsorption energy per molecule is:

$$\bar{E}_{diss} = \frac{E_{slab}(n(H,OH)) - E_{slab} - n \times E^{\infty}_{H_2O}}{n} \qquad (3)$$

where $E_{slab}(n(H,OH))$ is the total energy of a slab with n dissociated water molecules on the (1 x 3) surface.

3 Results and Discussion

3.1 Single water molecule interaction

In table 1, we list the molecular adsorption and dissociative adsorption energies we calculate for a perfect and a defective surface. The interaction of a single water molecule with a perfect and a defective TiO_2 surface is a reference system, which has been discussed in several DFT-based papers [12,14,15]. While the energy profile of the water molecule decomposition is largely endothermic on the perfect TiO_2 surface, the presence of a subsurface oxygen vacancy (as defined in Figure 1) has led to contrasting results, showing slight endothermic [14] or clear exothermic profiles [12,15], as seen in Table 1. The issue behind the

differences between the four results presented in table 1 lies in the stability of the subsurface oxygen vacancy. In Ref. [14], the oxygen vacancy remains stable, leading to an endothermic reaction pathway for dissociation of H_2O.

Table 1: Comparison of molecular and dissociative adsorption energies of a single water molecule on perfect and defective anatase (101) surfaces

Source	perfect surface		defective surface	
	$\bar{E}_{ads}$ (eV)	$\bar{E}_{diss}$ (eV)	$\bar{E}_{ads}$ (eV)	$\bar{E}_{diss}$ (eV)
This work	-0.81	-0.42	-0.99	-2.40
Ref 12	-0.70	-0.32	-0.85	-1.83
Ref 14	-0.72	-0.34	-1.01	-0.70
Ref 15	--	--	-0.84	- 1.59

Figs 2(a) – (c) show the molecular adsorption, metastable state of dissociative adsorption, and final state of dissociative adsorption of a water molecule on a defective surface, respectively. The oxygen atoms labeled 1, 2, and 3 in Fig 2(a) are involved the migration of the subsurface V_O towards the surface, and the arrows in Fig 2(b) show the movement of each atom during the migration. In agreement with Refs. [12 and 15], these figures show that the subsurface V_O migrates towards the surface as the water molecule dissociates, according to the following process: (i) after adsorption, reconstruction around the vacancy (V_O) is operating with the oxygen atom labeled 1 moving towards the vacancy site, in a bridge site situation between two Ti atoms (Fig. 2(a)); (ii) as the water molecule dissociates, 1 relaxes back downwards to its stoichiometric crystal position, while oxygen 2 migrates to occupy the initial V_O site. At this stage the vacancy is located immediately below the surface, *i.e.* in the third oxygen layer; 3 then moves downwards, towards the initial position occupied by oxygen 2 before its migration, oxygen 3 stabilizes as a bridge site, extending the defect site to two oxygen vacancy sites on the surface and immediate subsurface from either side of the oxygen 3 atom, as seen in Fig. 2(b). The structure in Fig. 2(b) is a metastable state and after overcoming another activation barrier the hydroxyl group attached to the surface migrates to annihilate the vacancy defect site as described in (ii) results in a final stable state as shown in Fig. 2c.

In Fig. 3, we present the energy pathway for the entire dissociation process of an adsorbed water molecule, accompanied with the migration of the V_O to the surface from the structure in Fig. 2a to the structure in Fig.

2c. The limiting step is the splitting of the adsorbed water molecule into a hydrogen atom, which binds to an oxygen atom on the surface, and a hydroxyl group which remains attached to the Ti atom. The energy barrier of 0.33 eV between the metastable and final states in Figs 2(b) and (c) respectively is the energy needed to move the hydroxyl group towards the surface V_O shown in Fig. 2(b). The entire process is exothermic, releasing a total of 1.41 eV, and has a low barrier of 0.35 eV.

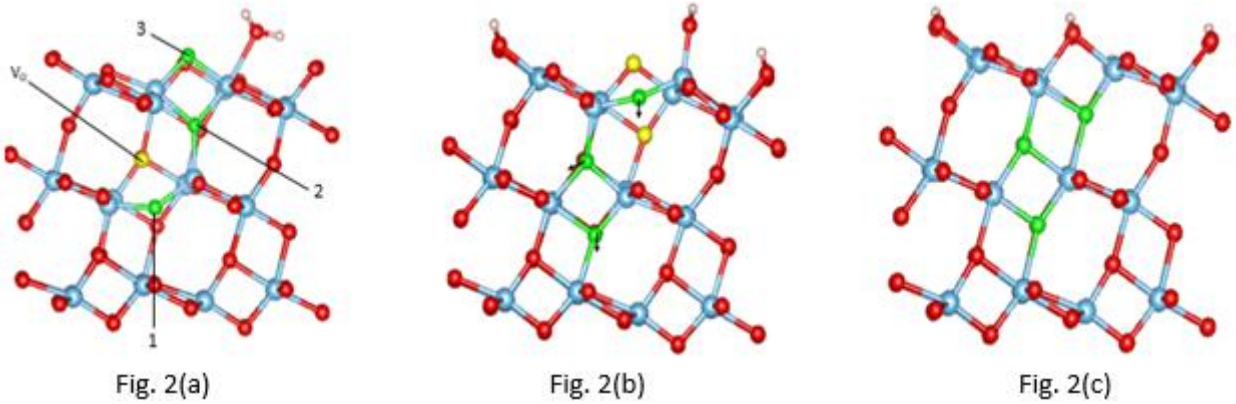

Fig. 2(a) Fig. 2(b) Fig. 2(c)

Figure 2: Diagrams of (a) molecular adsorption (b) metastable state of dissociative adsorption, and (c) final state of dissociative adsorption of a single water molecule on the defective surface. Oxygen atoms associated with vacancy migration are colored green and labeled 1, 2, and 3, while position of V_O is shown in yellow. Cyan: Ti atom; red: O atom; white: H atom

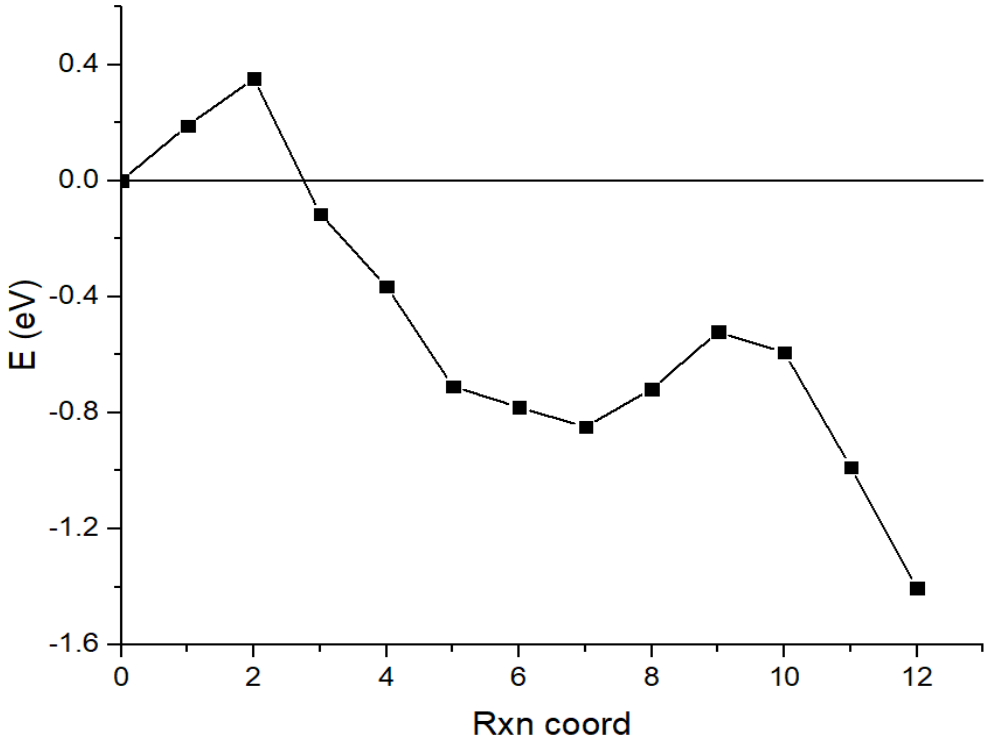

Fig.3 Energy pathway for the dissociation of an adsorbed water molecule on the defective surface, starting from the structure shown in Fig. 2(a) and ending with the structure in Fig. 2(c). The limiting step is the splitting of the adsorbed water molecule to H and OH, with a kinetic barrier of 0.35 eV.

3.2 Increasing Water Coverage

Fig. 4 shows a perfect surface fully saturated with six water molecules adsorbed via the six Ti_{5c} atoms on the surface (two adjacent rows of three Ti atoms each), which is equivalent to 1 ML coverage. Starting with a single water molecule on the surface, we found that the incremental adsorption energy for each additional water molecule was dependent on the Ti_{5c} atom to which it is attached. The lowest adsorption energies were obtained when water molecules were attached to neighboring Ti_{5c} atoms along the [010] direction. Using the most favorable adsorption energies for each additional molecular water adsorption, surface sites were therefore filled by adding a water molecule to each Ti_{5c} along the [010] direction, row by row. We calculated the energy required for the incremental adsorption of water molecules (molecular adsorption), using equation (1).

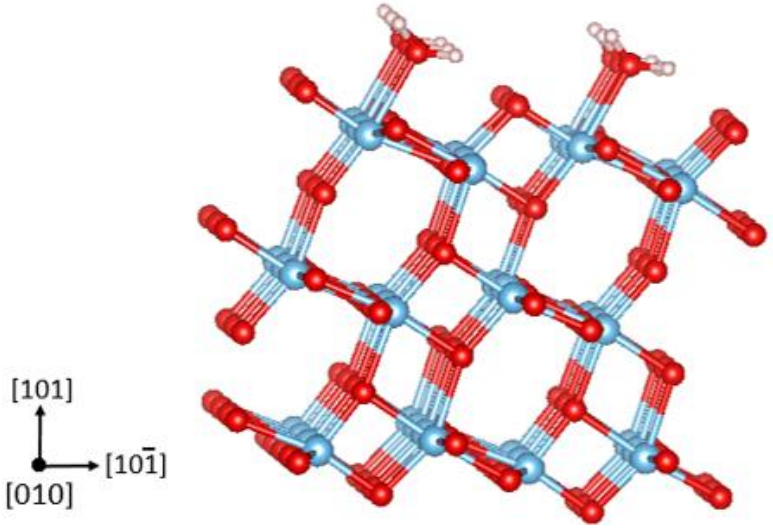

Figure 4: Ball and stick model of the stoichiometric TiO_2 anatase (101) slab, covered with 1 ML of adsorbed water molecules. Titanium atoms are cyan, oxygen atoms are red, and hydrogen atoms are white.

Table 2: Incremental non-dissociative adsorption energies of water molecules on both stoichiometric and defective TiO_2 anatase (101) surfaces

Coverage (n)	$\Delta E_{ads,n}$ **(eV)**	
	stoichiometric	defective

1 (16.7%)	-0.81	-0.99
2 (33.3%)	-0.91	-0.85
3 (50%)	-0.86	-0.96
4 (66.7%)	-0.80	-0.82
5 (83.3%)	-0.65	-0.87
6 (100%)	-0.82	-0.80

The calculated values of incremental adsorption energy on both surfaces, up to 1 ML coverage, are shown in table 2. The results show that 1 ML coverage with adsorbed water molecules is possible on both stoichiometric and defective surfaces since the successive adsorption energies at all levels of coverage are negative. The adsorption energy on the stoichiometric surface ranges from -0.64 eV to -0.91 eV, while on the defective surface, the values vary between -0.80 eV and -0.99 eV. Overall, molecular adsorption is more exothermic on the defective surface than on the perfect surface. Our results for the stoichiometric surface agree with previously published results for a similar (1 x 3) surface slab showing successive adsorption energies between -0.70 eV and -0.85 eV [20], and also agree with experimental results [25].

In Table 3, we show the effect of the subsurface V_O on the energy required for dissociation of adsorbed water molecules on the slab surface at different levels of coverage, with a comparison to the adsorption on the perfect surface. To compare, we calculate the adsorption energy per molecule for each type of adsorption, using equation (3). For a stoichiometric surface, molecular adsorption is always energetically more favorable than dissociative adsorption at all levels of coverage with water molecules. While non-dissociative adsorption energy is stable with increasing coverage, dissociative adsorption energy slightly increases (more than 0.1 eV gain). For a defective surface, the energy released on dissociative adsorption of the first water molecule on the surface is 2.40 eV, relative to the infinitely separated water molecule and slab, compared to the 0.99 eV released on molecular adsorption. In other words, 1.41 eV is released when an isolated water molecule adsorbed on the surface dissociates. A similar exothermic profile persists on the defective surface for the first four adsorbed water molecules, which corresponds to 2/3 ML coverage. At 2/3 ML coverage (coverage n = 4), the energy released per adsorbed water molecule drops down to 0.09 eV. Beyond this level of coverage, non-dissociative molecular adsorption becomes more favorable, similar to the dissociation on perfect surfaces.

Table 3: Values of average molecular and dissociative adsorption energies on stoichiometric and defective surfaces

	perfect surface		**defective surface**	
Coverage (n)	**E_{ads} (eV)**	**E_{diss} (eV)**	**E_{ads} (eV)**	**E_{diss} (eV)**

1 (16.7%)	-0.81	-0.42	-0.99	-2.40
2 (33.3%)	-0.86	-0.46	-0.92	-1.34
3 (50%)	-0.86	-0.41	-0.93	-1.08
4 (66.7%)	-0.85	-0.50	-0.91	-1.00
5 (83.3%)	-0.81	-0.55	-0.90	-0.66
6 (100%)	-0.81	-0.56	-0.88	-0.61

Fig. 5 shows how the energy required to dissociate each adsorbed water molecule (ΔE_{diss}/molecule) changes with the number of adsorbed molecules for both the defective and the stoichiometric surface. The presence of a subsurface V_O enhances dissociation of adsorbed water molecules up to 2/3 ML (four water molecules). When coverage increases to 5/6 and 6/6 water molecules, the energy required for dissociation of each adsorbed water molecule on both surfaces is more than 0.2 eV, clearly illustrating the switch from an exothermic to an endothermic profile as coverage increases beyond 2/3 coverage.

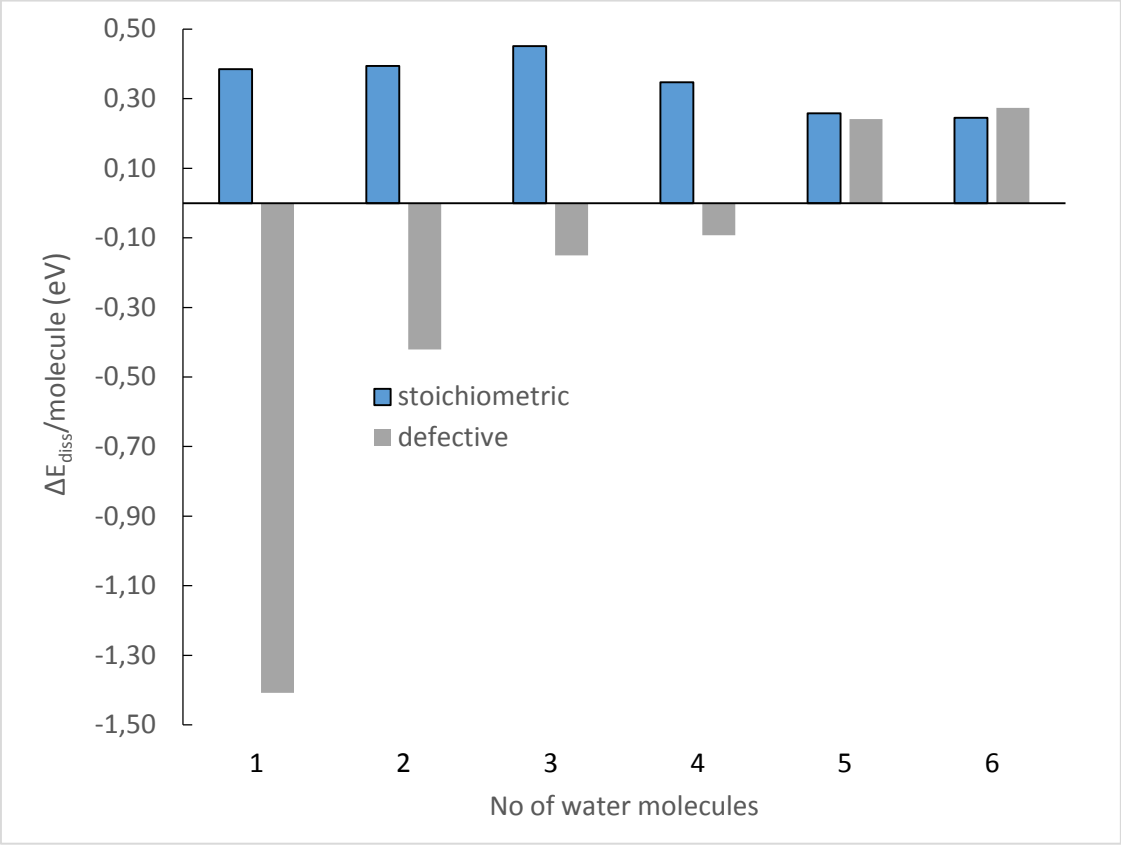

Figure 5: Energy required (per molecule) to dissociate an adsorbed water molecule on both stoichiometric and defective surfaces, at different levels of coverage.

Fig. 6 shows the results of charge density difference analysis, which illustrates the distribution of the excess charge in the system due to the oxygen vacancy. The position of the vacancy is colored green, indicating a loss of charge while the regions gaining charge, colored yellow, are around Ti atoms. The significant reduction observed in the dissociative adsorption energy can be attributed to the charge distribution pattern seen in Fig. 6. Out of the six surface Ti_{5c} atoms to which water molecules are attached, the only Ti_{5c} with a significant concentration of excess charge is the one to which the first water molecule is adsorbed. The excess charge facilitates a stronger bond between the Ti_{5c} and the oxygen atom of the water molecule. The resulting weakening of O-H bonds thereby enhances the dissociation of the water molecule into H and OH species. The system is stabilized by the dissociation of the water molecule, leading to the relatively large energy gain of 1.41 eV upon dissociation.

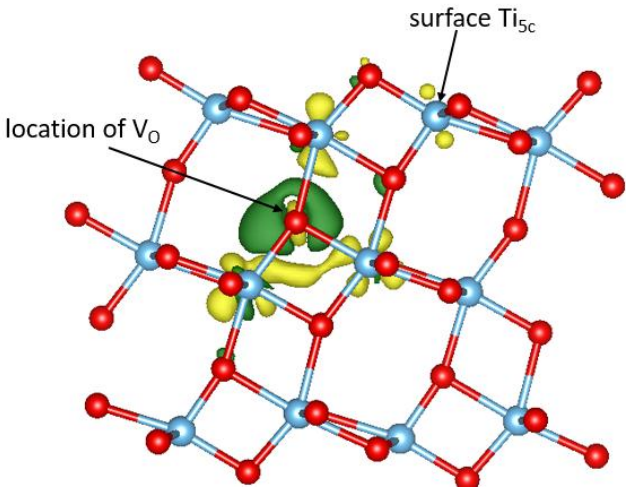

Figure 6: Charge density difference analysis showing the net flow of charge due to the creation of a subsurface vacancy in the slab. Charge flows from regions highlighted in green to regions highlighted in yellow.

Figs. 7(a) to (c) show the initial, molecular adsorption state in the case of two, five, and six water molecules on the defective surface. Three distinct behaviors of the subsurface V_O can be observed in Fig. 7. For the case of two molecules, the structural changes are similar to the one obtained with a single water molecule dissociating. As the water molecules dissociate, the oxygen vacancy migrates to the surface, and the local reconstruction around the vacancy involves the oxygen atom labeled O_B moving to occupy the vacancy position. O_C moves downwards to the initial position of O_B, and O_w, the oxygen atom of a dissociated water molecule relaxes to annihilate the surface vacancy, as shown in Fig. 7(d). The molecular and dissociative adsorptions for three and four water molecules are shown in Figs. S1 (a) to (d). Even though the average dissociative adsorption energy drops by 1.32 eV as coverage increases from one to four molecules, the final structure at the vacancy site remains similar.

At high coverage (5/6 water molecules), the defect structure modifies as shown in Fig. 7(e). O_B moves towards the subsurface V_O site and occupies the vacancy, and O_C moves towards the subsurface vacancy created at the initial position of O_B but does not occupy the vacancy. In the final dissociative state, the vacancy has migrated closer to the surface as seen in Fig. 7(e). Interestingly, at coverage n = 5, the surface O_{2c} that connects to the defect site is now turning into a bridged OH configuration, due to the bonding with the hydrogen atom following the dissociation of the water molecule. While the original defect site remains similar to the preceding n = 4 coverage, the energy budget becomes endothermic. The process is even more accentuated at full coverage. All surface O_{2c} become saturated as bridged OH configurations. In the final configuration for n = 6, the subsurface vacancy remains stable, roughly in its original configuration, before dissociation, Fig 7(f). Fig. 4 shows that dissociation of each adsorbed water molecule on the defective surface requires 0.27 eV, while 0.24 eV is required for dissociation on the perfect surface. The quantitative results and the reconstruction patterns observed confirm the role of the vacancy migration to the exothermic/endothermic transition of the dissociation pathway.

We further introduced a second subsurface V_O to investigate the effect of vacancy concentration or the formation of a subsurface vacancy cluster, which has been observed experimentally [38], on the dissociation of adsorbed water at 5/6 and 1ML coverage. We considered two possible cases: separated vacancies and a cluster of vacancies. The results, as presented in Table S1 and Figs S2-S4 show that the dissociative adsorption remains endothermic relative to molecular adsorption at these levels of coverage. The energy required to dissociate a molecule at 5/6 ML coverage reduces for both slabs with two vacancies. For the slab with separated vacancies, the final structure is further stabilized because a hydrogen bond forms between the hydrogen atom of a dissociated water molecule and a neighboring oxygen atom as seen in Fig S3(c), and the energy required for dissociation reduces from 0.24 eV in the single V_O structure to 0.09 eV. In the slab with a cluster, the required energy for dissociation is smaller: 0.05 eV, due to the relaxation of the two-fold coordinated (O_{2c}) oxygen atom on the surface, as illustrated in Fig S4(c). A recent study on the more reactive but less stable (001) surface of anatase also shows that water splitting remains endothermic in the presence of two surface oxygen vacancies[39], but the comparison between that investigation and this work is limited because of the differences between the facets of anatase studied and the positions of the oxygen vacancies considered. The diagrams of the relaxed structures in Figs S3 and S4 are similar to those obtained for a single V_O. There is a partial migration of one V_O towards the surface at 5/6 ML coverage, while no significant V_O migration is seen at 1 ML coverage for both types of double V_O.

Previous investigations with only one adsorbed water molecule have concluded that the presence of a subsurface vacancy enhances dissociation by either reducing the energy barrier required for dissociation while the dissociation becomes less endothermic [14], or changing the dissociation step to an exothermic

process accompanied by a reduced dissociation barrier [12,15]. But the described change in the energy profile during dissociation is rather local, and coverage dependent. Our results indicate that at 1 ML full coverage and in the presence of either one or two subsurface V_Os, dissociation of adsorbed water molecules is still endothermic, and the vacancy has no catalytic effect on the splitting of water molecules adsorbed on the defective surface.

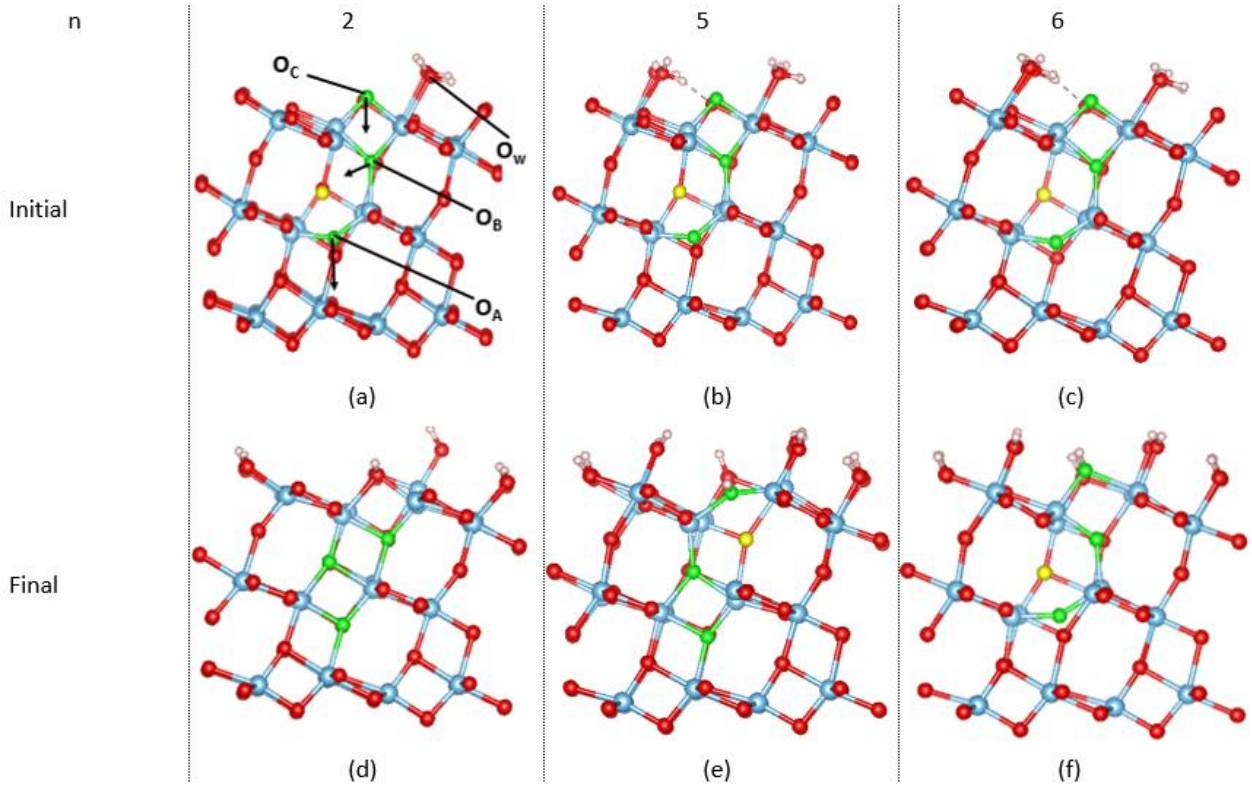

Figure 7: Diagrams of molecular (a) – (c) and dissociative (d) – (f) adsorption of water molecules on the defective surface for 2/6, 5/6, and 6/6 ML coverages. Oxygen atoms of TiO_2 slab associated with vacancy migration (O_A, O_B, and O_C) are colored green, while position of an oxygen vacancy is shown in yellow. O_w is an oxygen atom of a water molecule. The arrows in Fig. 7(a) show the respective movement of the O atoms during reconstruction and vacancy migration. Cyan: Ti atom; red: O atom; white: H atom

The reported values of dissociative adsorption energies at different levels of coverage and the movement of atoms leading to the migration of the subsurface V_O described above show that the enhancement of the dissociation of adsorbed water molecules by a subsurface vacancy is dependent on the presence of an under-coordinated surface oxygen atom (O_{2c}), within the vicinity of the subsurface vacancy. As shown in Figs. 7(a) and (d), the movements of oxygen atoms O_B and O_C enable the subsurface V_O to migrate towards the surface. When O_C is fully coordinated, as seen in Figs. 7(e) and (f), the vacancy remains in a subsurface position and the splitting of the adsorbed water molecule is endothermic, making it unlikely to take place.

4 Conclusions

We have investigated the role of a subsurface oxygen vacancy in the splitting of chemisorbed water molecules on the anatase (101) surface at different levels of coverage, up to 1 ML coverage. Up to 2/3 ML coverage, the subsurface V_O enhanced the splitting chemistry, making dissociative adsorption more thermodynamically favorable than molecular adsorption. In all instances, this enhancement was accompanied by a migration of the V_O towards the surface, and the migration was made possible by the presence of an under-coordinated surface oxygen atom near the vacancy. In the absence of such a surface atom, and especially at full ML coverage, molecular adsorption is more thermodynamically favorable than dissociative adsorption on the defective surface with a subsurface V_O, similar to the results obtained for a stoichiometric surface.

Our findings indicate that contrary to previous findings, subsurface V_O are unlikely to catalyze water splitting. While a subsurface V_O enhances the photo-splitting on a surface with a defect, it only does this when not accounting for water coverage.

Acknowledgements

The authors acknowledge the Texas Advanced Computing Center (TACC) at The University of Texas at Austin for providing HPC resources that have contributed to the research results reported within this paper. URL: http://www.tacc.utexas.edu

References

[1] U. Diebold, The surface science of titanium dioxide, Surf. Sci. Rep. 48 (2003) 53–229. https://doi.org/10.1016/S0167-5729(02)00100-0.

[2] M.R. Hoffmann, S.T. Martin, W. Choi, D.W. Bahnemann, Environmental Applications of Semiconductor Photocatalysis, Chem. Rev. 95 (1995) 69–96. https://doi.org/10.1021/cr00033a004.

[3] A. Fujishima, K. Honda, Electrochemical Photolysis of Water at a Semiconductor Electrode, Nature. 238 (1972) 37–38. https://doi.org/10.1038/238037a0.

[4] M.-I. Mendoza-Diaz, J. Cure, M.D. Rouhani, K. Tan, S.-G. Patnaik, D. Pech, M. Quevedo-Lopez, T. Hungria, C. Rossi, A. Estève, On the UV–Visible Light Synergetic Mechanisms in Au/TiO2 Hybrid Model Nanostructures Achieving Photoreduction of Water, J. Phys. Chem. C. 124 (2020) 25421–25430. https://doi.org/10.1021/acs.jpcc.0c08381.

[5] X. An, C. Hu, H. Liu, J. Qu, Hierarchical Nanotubular Anatase/Rutile/TiO2(B) Heterophase Junction with Oxygen Vacancies for Enhanced Photocatalytic H2 Production, Langmuir. 34 (2018) 1883–1889. https://doi.org/10.1021/acs.langmuir.7b03745.

[6] A.A. Ismail, D.W. Bahnemann, Photochemical splitting of water for hydrogen production by photocatalysis: A review, Sol. Energy Mater. Sol. Cells. 128 (2014) 85–101. https://doi.org/10.1016/j.solmat.2014.04.037.

[7] R. Asahi, T. Morikawa, T. Ohwaki, K. Aoki, Y. Taga, Visible-Light Photocatalysis in Nitrogen-Doped Titanium Oxides, Science. 293 (2001) 269–271. https://doi.org/10.1126/science.1061051.

[8] S.-H. Liu, H.-R. Syu, One-step fabrication of N-doped mesoporous TiO2 nanoparticles by self-assembly for photocatalytic water splitting under visible light, Appl. Energy. 100 (2012) 148–154. https://doi.org/10.1016/j.apenergy.2012.03.063.
[9] T. Ohno, T. Mitsui, M. Matsumura, Photocatalytic Activity of S-doped TiO2 Photocatalyst under Visible Light, Chem. Lett. 32 (2003) 364–365. https://doi.org/10.1246/cl.2003.364.
[10] E. Coy, K. Siuzdak, I. Grądzka-Kurzaj, S. Sayegh, M. Weber, M. Ziółek, M. Bechelany, I. Iatsunskyi, Exploring the effect of BN and B-N bridges on the photocatalytic performance of semiconductor heterojunctions: Enhancing carrier transfer mechanism, Appl. Mater. Today. 24 (2021) 101095. https://doi.org/10.1016/j.apmt.2021.101095.
[11] J. Cure, K. Cocq, A. Mlayah, T. Hungria, P. Alphonse, Y.J. Chabal, V. Maraval, R. Chauvin, A. Estève, C. Rossi, A triptych photocatalyst based on the Co-Integration of Ag nanoparticles and carbo-benzene dye into a TiO2 thin film, Int. J. Hydrog. Energy. 44 (2019) 26347–26360. https://doi.org/10.1016/j.ijhydene.2019.08.126.
[12] G. Fisicaro, S. Filice, S. Scalese, G. Compagnini, R. Reitano, L. Genovese, S. Goedecker, I. Deretzis, A. La Magna, Wet Environment Effects for Ethanol and Water Adsorption on Anatase TiO2 (101) Surfaces, J. Phys. Chem. C. 124 (2020) 2406–2419. https://doi.org/10.1021/acs.jpcc.9b05400.
[13] X. Lang, Y. Liang, L. Sun, S. Zhou, W.-M. Lau, Interplay between Methanol and Anatase TiO2(101) Surface: The Effect of Subsurface Oxygen Vacancy, J. Phys. Chem. C. 121 (2017) 6072–6080. https://doi.org/10.1021/acs.jpcc.6b11356.
[14] U. Aschauer, Y. He, H. Cheng, S.-C. Li, U. Diebold, A. Selloni, Influence of Subsurface Defects on the Surface Reactivity of TiO2: Water on Anatase (101), J. Phys. Chem. C. 114 (2010) 1278–1284. https://doi.org/10.1021/jp910492b.
[15] Y. Li, Y. Gao, Interplay between Water and TiO 2 Anatase (101) Surface with Subsurface Oxygen Vacancy, Phys. Rev. Lett. 112 (2014) 206101. https://doi.org/10.1103/PhysRevLett.112.206101.
[16] A. Vittadini, A. Selloni, F.P. Rotzinger, M. Grätzel, Structure and Energetics of Water Adsorbed at TiO 2 Anatase \(101\) and \(001\) Surfaces, Phys. Rev. Lett. 81 (1998) 2954–2957. https://doi.org/10.1103/PhysRevLett.81.2954.
[17] A. Vittadini, M. Casarin, A. Selloni, Chemistry of and on TiO2-anatase surfaces by DFT calculations: a partial review, Theor. Chem. Acc. 117 (2007) 663–671. https://doi.org/10.1007/s00214-006-0191-4.
[18] M. Lazzeri, A. Vittadini, A. Selloni, Structure and energetics of stoichiometric TiO 2 anatase surfaces, Phys. Rev. B. 63 (2001) 155409. https://doi.org/10.1103/PhysRevB.63.155409.
[19] C. Arrouvel, M. Digne, M. Breysse, H. Toulhoat, P. Raybaud, Effects of morphology on surface hydroxyl concentration: a DFT comparison of anatase–TiO2 and γ-alumina catalytic supports, J. Catal. 222 (2004) 152–166. https://doi.org/10.1016/j.jcat.2003.10.016.
[20] H. Valdés, L.M. Molina, J.A. Alonso, Water adsorption and dissociation on gold catalysts supported on anatase-TiO2(101), Appl. Surf. Sci. 487 (2019) 244–252. https://doi.org/10.1016/j.apsusc.2019.04.249.
[21] Y.-F. Li, Z.-P. Liu, L. Liu, W. Gao, Mechanism and Activity of Photocatalytic Oxygen Evolution on Titania Anatase in Aqueous Surroundings, J. Am. Chem. Soc. 132 (2010) 13008–13015. https://doi.org/10.1021/ja105340b.
[22] Y. He, O. Dulub, H. Cheng, A. Selloni, U. Diebold, Evidence for the Predominance of Subsurface Defects on Reduced Anatase TiO 2 (101), Phys. Rev. Lett. 102 (2009) 106105. https://doi.org/10.1103/PhysRevLett.102.106105.
[23] H. Cheng, A. Selloni, Energetics and diffusion of intrinsic surface and subsurface defects on anatase TiO2(101), J. Chem. Phys. 131 (2009) 054703. https://doi.org/10.1063/1.3194301.
[24] A. Tilocca, A. Selloni, Vertical and Lateral Order in Adsorbed Water Layers on Anatase TiO2(101), Langmuir. 20 (2004) 8379–8384. https://doi.org/10.1021/la048937r.
[25] Y. He, A. Tilocca, O. Dulub, A. Selloni, U. Diebold, Local ordering and electronic signatures of submonolayer water on anatase TiO2(101), Nat. Mater. 8 (2009) 585–589. https://doi.org/10.1038/nmat2466.
[26] J.P. Perdew, K. Burke, M. Ernzerhof, Generalized Gradient Approximation Made Simple, Phys. Rev. Lett. 77 (1996) 3865–3868. https://doi.org/10.1103/PhysRevLett.77.3865.
[27] G. Kresse, J. Furthmüller, Efficient iterative schemes for ab initio total-energy calculations using a plane-wave basis set, Phys. Rev. B. 54 (1996) 11169–11186. https://doi.org/10.1103/PhysRevB.54.11169.

[28] G. Kresse, J. Furthmüller, Efficiency of ab-initio total energy calculations for metals and semiconductors using a plane-wave basis set, Comput. Mater. Sci. 6 (1996) 15–50. https://doi.org/10.1016/0927-0256(96)00008-0.
[29] G. Kresse, J. Hafner, Ab initio molecular dynamics for liquid metals, Phys. Rev. B. 47 (1993) 558–561. https://doi.org/10.1103/PhysRevB.47.558.
[30] G. Kresse, J. Hafner, Ab initio molecular-dynamics simulation of the liquid-metal--amorphous-semiconductor transition in germanium, Phys. Rev. B. 49 (1994) 14251–14269. https://doi.org/10.1103/PhysRevB.49.14251.
[31] G. Kresse, D. Joubert, From ultrasoft pseudopotentials to the projector augmented-wave method, Phys. Rev. B. 59 (1999) 1758–1775. https://doi.org/10.1103/PhysRevB.59.1758.
[32] P.E. Blöchl, Projector augmented-wave method, Phys. Rev. B. 50 (1994) 17953–17979. https://doi.org/10.1103/PhysRevB.50.17953.
[33] S. Grimme, J. Antony, S. Ehrlich, H. Krieg, A consistent and accurate ab initio parametrization of density functional dispersion correction (DFT-D) for the 94 elements H-Pu, J. Chem. Phys. 132 (2010) 154104. https://doi.org/10.1063/1.3382344.
[34] H. Jonsson, G. Mills, K.W. Jacobsen, Nudged elastic band method for finding minimum energy paths of transitions, in: Class. Quantum Dyn. Condens. Phase Simul., WORLD SCIENTIFIC, 1998: pp. 385–404. https://doi.org/10.1142/9789812839664_0016.
[35] X. Liu, J. Fu, Electronic and elastic properties of the tetragonal anatase TiO2 structure from first principle calculation, Optik. 206 (2020) 164342. https://doi.org/10.1016/j.ijleo.2020.164342.
[36] J.K. Burdett, T. Hughbanks, G.J. Miller, J.W. Richardson, J.V. Smith, Structural-electronic relationships in inorganic solids: powder neutron diffraction studies of the rutile and anatase polymorphs of titanium dioxide at 15 and 295 K, J. Am. Chem. Soc. 109 (1987) 3639–3646. https://doi.org/10.1021/ja00246a021.
[37] X. Wang, L. Zhang, Y. Bu, W. Sun, Interplay between invasive single atom Pt and native oxygen vacancy in anatase TiO2(1 0 1) surface: A theoretical study, Appl. Surf. Sci. 540 (2021) 148357. https://doi.org/10.1016/j.apsusc.2020.148357.
[38] M. Setvin, M. Schmid, U. Diebold, Aggregation and electronically induced migration of oxygen vacancies in TiO 2 anatase, Phys. Rev. B. 91 (2015) 195403. https://doi.org/10.1103/PhysRevB.91.195403.
[39] E. Mete, Ş. Ellialtıoğlu, O. Gulseren, D. Uner, Elucidating the Barriers on Direct Water Splitting: Key Role of Oxygen Vacancy Density and Coordination over PbTiO3 and TiO2, J. Phys. Chem. C. 125 (2021) 1874–1880. https://doi.org/10.1021/acs.jpcc.0c09685.